Bull. Chem. Soc. Jpn., 70, 719—726 (1997)

Headline Articles

Bethe Surface of Liquid Water Determined by Inelastic X-Ray Scattering Spectroscopy and Electron Correlation Effects

Noboru Watanabe, Hisashi Hayashi, and Yasuo Udagawa*

Research Institute for Scientific Measurements, Tohoku University, Katahira 2-1-1, Sendai 980-77

(Received December 16, 1996)

By means of inelastic X-ray scattering spectroscopy, the generalized oscillator strength (GOS) of liquid water has been experimentally determined over a range $0.69 \leqq q \leqq 3.59$ a.u., where q is the momentum transfer. The Bethe surface was constructed from the GOS, and the loss function, the dielectric response function, and the static structure factor were deduced. It was found that the GOS of liquid water is dominated by individual molecular properties over the q range studied, and that the static structure factor agrees quite well with a calculation including electron-electron correlation effects.

It has long been pointed out that the generalized oscillator strength (GOS) is of fundamental importance in understanding optical and dielectric properties of substances, as well as the interactions of matters with charged particles.[1,2] The GOS, $df(\boldsymbol{q},E)/dE$, is defined by Eq. 1 and can be determined from inelastic scattering experiments where momentum $\boldsymbol{q}$ and energy E are transferred.

$$\frac{df(\boldsymbol{q},E)}{dE} = \frac{E}{R(qa_0)^2}\sum_f \left|\left\langle f\left|\sum_{j=1}^{N}\exp(i\boldsymbol{q}\cdot\boldsymbol{r}_j)\right|i\right\rangle\right|^2. \quad (1)$$

Here $|i>$ and $|f>$ indicate the initial and final state, a_0 the Bohr radius, $\boldsymbol{r}_j$ the coordinate of the j-th electron, and R the Rydberg constant. The GOS is a normalized quantity and can be made absolute by applying the Bethe sum rule, Eq. 2:

$$\int_0^\infty \frac{df(\boldsymbol{q},E)}{dE}dE = N, \quad (2)$$

where N is the total number of electrons in the target. At the limit $q\rightarrow 0$, GOS is reduced to the optical oscillator strength. The magnitude of q depends on the wavelength λ of the incident radiation and on the scattering angle θ according to $q=(4\pi/\lambda)\sin(\theta/2)$.

From GOS, various properties of matters can be extracted: dielectric response function, stopping power, polarizability, and so on. In particular, GOS can be used to calculate the X-ray incoherent scattering factor which is related to the electron pair correlation function and is a very correlation-sensitive quantity.[3] The global variation of a GOS over extended ranges of energy and momentum transferred is best illustrated in a form called the Bethe surface,[1] which contains all the information about the interactions between matters and electrons or photons. Although the significance of the Bethe surface has often been stressed,[4] few experimental determination have been reported.

Election energy loss spectroscopy (EELS) has been employed in previous GOS studies, and because of the nature of the method, only gas phase atoms or molecules have been the main concern.[5—16] Several properties of matters derived from GOS, such as stopping powers and dielectric response functions, are, however, more important for aggregates rather than for low pressure gases. Inelastic X-ray scattering spectroscopy (IXSS) is an alternative to obtain GOS. The double differential cross section of the inelastic X-ray scattering ($d^2\sigma/d\Omega dE$) is expressed by the dynamic structure factor $S(\boldsymbol{q},E)$, which is related to $df(\boldsymbol{q},E)/dE$, as is evident from the following equations:[17]

$$\frac{\partial^2\sigma}{\partial\Omega\partial E} = (\boldsymbol{e}_0\cdot\boldsymbol{e}_1)r_0^2\left(\frac{E_1}{E_0}\right)S(\boldsymbol{q},E)$$
$$= (\boldsymbol{e}_0\cdot\boldsymbol{e}_1)r_0^2\left(\frac{E_1}{E_0}\right)\sum_f\left|\left\langle f\left|\sum_{j=1}^{N}\exp(i\boldsymbol{q}\cdot\boldsymbol{r}_j)\right|i\right\rangle\right|^2. \quad (3)$$

Here $\boldsymbol{e}_0$ and $\boldsymbol{e}_1$ are the polarization vectors, E_0 and E_1 are the energies of incident and scattered X-ray photons, and r_0 is the classical electron radius. The equation above is quite general, but depending on the magnitude of qr, IXSS can be classified into several types. In the case where the X-ray photon energy is high, that is, q is very large and thus $qr \gg 1$, the IXSS is the well known Compton scattering;[18] binding energies of electrons can be neglected and the spectra are approximated by symmetric parabolas. On the other hand, if core electrons, whose spatial spreads are small, are involved in the transition

and consequently $qr \ll 1$, the IXSS is called X-ray Raman scattering.[19—21] The binding energy can not be neglected but effects of momentum transfer can, and the spectrum shows fine structures similar to those observed in the corresponding X-ray absorption. In the IXSS experiment reported here, X-rays of about 2 Å are scattered by valence electrons of H_2O and thus $qr \approx 1$. Accordingly both the binding energy and momentum transfer should be taken into consideration, providing GOS which depends on q as well as on E.

A study of GOS by IXSS has several advantages as well as disadvantages. It can be applied to condensed phases and is free from several experimental difficulties with which EELS is plagued: multiple scatterings, a need of vacuum, and charge up phenomena. Studies by IXSS aiming to determine GOS are, however, few, the reason being weak scattering intensities. Recent developments of synchrotron radiation (SR) sources have provided a possibility to extend IXSS to obtain GOS of molecules and solids. So far IXSS of some elementary solids such as Li, C, Al, and Si have been reported and analyzed in terms of the homogeneous electron gas models.[22—25] For molecules which consist of a limited number of atoms, more accurate ab initio calculations can be made to analyze data.

The purpose of the present study is to establish a method to determine GOS of liquids by IXSS and to show what kind of molecular properties can be extracted therefrom. The GOS of liquid water is determined up to 200 eV over a q range between 0.69 and 3.59 a.u. and the Bethe surface is constructed. It is compared with gas phase values reported by Lassettre and White[5] from EELS measurements. Then the dielectric response function is deduced and the experimentally determined X-ray incoherent scattering factor (static structure factor) is compared with theoretical values calculated with correlated or uncorrelated wavefunctions. This study makes it experimentally certain that IXSS is a very effective and unique means to determine GOS and has wide applications.

Experimental and Data Processing

Inelastic X-ray scattering measurements were performed at a multipole wiggler line, BL-16A, of the Photon Factory, KEK, Tsukuba. The beam line consists of a collimating mirror, a sagittally focusing double Si(111) crystal monochromator, and a vertically focusing mirror.[26] The flux is believed to be about 10^{12} photons/s, and the spectral width measured was better than 1.0 eV at 7 keV.

In order to avoid scatterings from window materials, no liquid cell was used. Instead, the incident X-rays were focused to a distilled water jet expanded from a nozzle (0.5×5 mm) at the center of a chamber filled with He gas. Two apertures, 2.8×5.5 mm and 4.6×8.6 mm in size, were placed at 25 and 40 mm from the sample position to block parasitic scatterings.

The scattered X-rays were vertically focused and horizontally dispersed with respect to the scattering plane. A cylindrically bent 50×50 mm Ge(440) crystal having a 550 mm radius of curvature is employed in a polychromator schematically shown in Fig. 1. In this configuration, a 150 eV bandpass centered at about 7270 eV was collected into a defined angle of 58.5±2.0°. The energy resolution is determined by the illuminated sample volume and was around

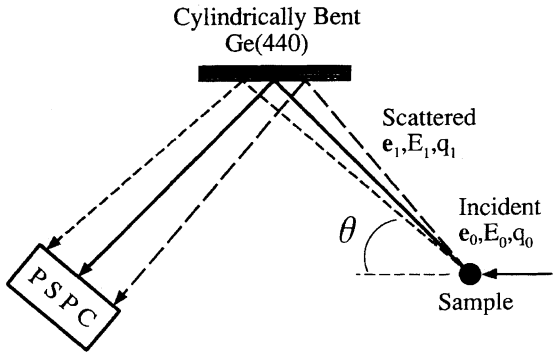

Fig. 1. A schematic of the experimental setup for the inelastic X-ray scattering. PSPC: position sensitive proportional counter.

2 eV from the FWHM of the elastic scattering line. The scattered X-rays were detected with a 100 mm long position-sensitive proportional counter (PSPC) combined with a multichannel analyzer (MCA). One channel of the MCA corresponds to about 0.26 eV at the center of the PSPC. For numerical analyses of the data, signals from every three channels were summed up and then processed.

The polychromator is separated from the sample chamber and detector with Kapton films and was evacuated. Typical data collection times were 3 h per spectrum, accumulating more than 5000 counts at the peak positions of the inelastic scattering spectra. The response function of the analyzer-detector combination as a function of scattered energy was determined by scanning the input energy while measuring the intensity of the elastic peak.

By varying the scattering angle θ from 20° to 130°, a momentum transfer range $0.69 \leq q \leq 3.59$ a.u. is covered. In this configuration, an energy-loss spectrum can be obtained simultaneously, while the momentum transferred differs slightly depending on the energy-loss. The difference in the momentum transferred at the two edges of the PSPC varies from ±0.04 (q=3.59) to ±0.07 (q=0.69) a.u. Three different excitation energies, 7271, 7385, and 7503 eV, were chosen to get scattering spectra over $-100 \leq E \leq 250$ eV. For $q > 2.9$ a.u. an excitation energy 7625 eV was also used to cover the spectra up to 420 eV.

The measured spectra were transformed to GOS in the following manner. First, a constant background signal was estimated from the count rate on the high energy side of the elastic line and was subtracted. Then, after being corrected by the response function of the analyzer-detector combination, the elastic scattering was removed by fitting it to a symmetrical function, resulting in a corrected inelastically scattered spectrum. Figure 2 shows raw data obtained at scattering angles of 20 and 65° before and after the subtraction of the elastic scattering. Finally, the inelastic scattering spectra are transformed to absolute $S(\boldsymbol{q},E)$ or GOS by the use of the Bethe sum rule.

In the normalization procedure, the data were least-squares fitted to the function A/E^B over the energy region 100—250 eV for q less than 2.9 a.u. and 300—420 eV for q larger than 2.9 a.u., and extrapolated to infinity. B varied from 2.5 to 4. The total area was then normalized to a value of 8.34, which corresponds to the total number of valence electrons (8) plus a small estimated correction for the Pauli-excluded transition from the oxygen K shell to the already occupied valence shell orbitals.[27] The selected value 0.34 corresponds to that for Ne, which is isoelectronic with H_2O.

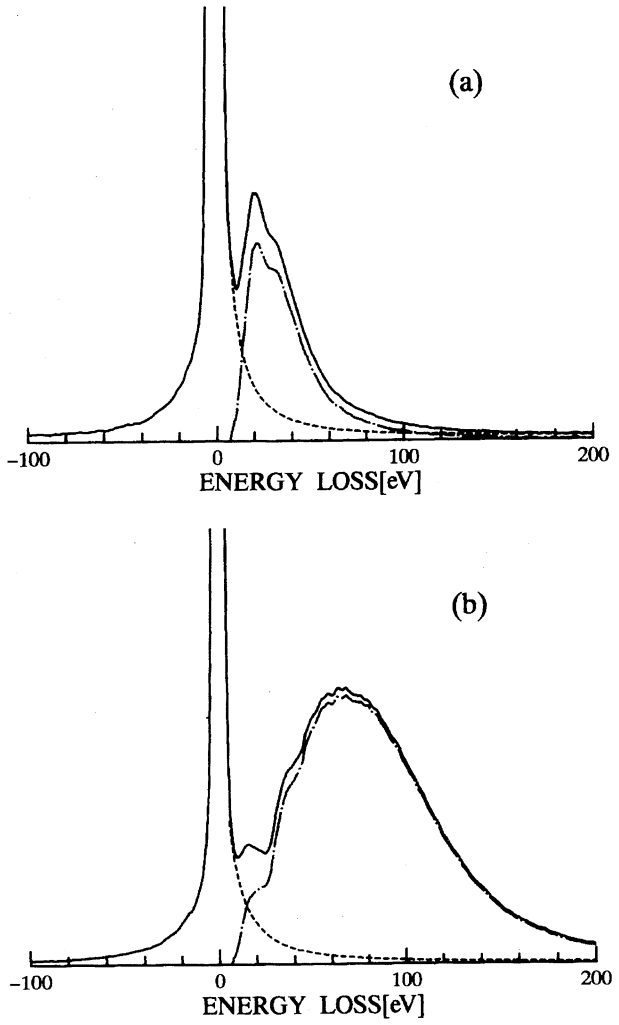

Fig. 2. Observed spectra after the subtraction of the constant background and the calibration by the response function of the analyzer-detector combination (solid lines), estimated elastic scatterings (dots), and the extracted inelastic scattering spectra (chains) at the scattering angle of 20° (q=0.69 a.u.) (a) and 65° (q=2.11 a.u.) (b).

Results and Discussion

Accuracy of the Data. Since the GOS is a normalized quantity, no absolute measurements of the scattering intensities as well as path length or sample concentration are required for its determination. What must be established is the accuracy of the relative intensities within a scattering spectrum, on which various factors exert influence. The statistical accuracy of the sums in the sum rules is small because of the large total number of signals accumulated. The subtraction of the elastic scattering line may introduce some errors, but as long as the assumption that it is symmetric is valid, the uncertainty can be neglected because of the high signal-to-noise ratio of the elastic scattering. In order to make use of the sum rule, the observed spectra were extrapolated to infinity by least-squares fitted to the function A/E^B. This may be another source of errors, but can also be neglected because the total contribution of the extrapolated part to the integral is at most 7%. Although Eq. 2 holds for constant momentum transfer, the momentum transfer in this experiment depends a little on the energy transferred. The effect caused by this is small, too, because GOS is a slowly varying function of q over the q range studied.

The reflectivity of the monochromator crystal depends on the wavelength of the X-rays, and the sensitivity of the PSPC may depend on the position. Both have been taken into consideration by the calibration using the response function of the analyzer-detector combination as is described in the experimental section. A correction for the energy dependence of the absorption of the sample is also included in the response function, because it was measured under the same experimental conditions using water jet as a scatterer.

The calibration by the use of the response function is based on the assumption that the intensity of the synchrotron radiation is constant within a narrow energy range (less than 150 eV) and during the scanning. Because the excitation energies employed are close to the peak energy of the multipole wiggler,[26] the intensity distribution is expected to be almost flat. Indeed, the intensity variation within a spectrum range used to determine a response function was measured to be less than 3%, the high energy side being more intense. The ring current decreased by about 2% during each measurement of a response function. Since the scanning is made toward the higher energy, the two effects partly cancel out each other; hence no correction was made in these regards. Although it is not possible to make a quantitative estimate of the accuracy of the present measurements, agreements of the final results with other studies described later strongly indicate that errors are insignificant.

Bethe Surface. Figure 3 shows normalized $S(q,E)$ spectra for several selected q values, where the measured $S(q,E)$ is spherically averaged owing to random orientation of molecules in liquids. At the lowest momentum transfer studied, namely q=0.69 a.u., a peak is observed at about 20 eV with a shoulder at 35 eV, which becomes the strongest peak at q=0.85 a.u. With increasing momentum transfer,

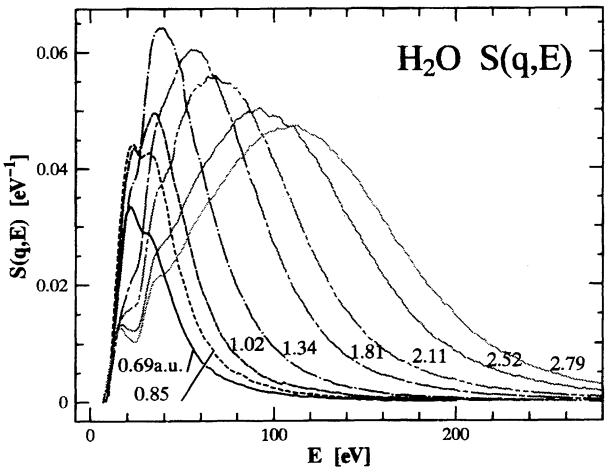

Fig. 3. Normalized $S(q,E)$ of liquid H_2O over a range $0.69 \leqq q \leqq 3.59$ a.u. Indicated in the figure are transferred momenta in a.u.

peak energies drift further to higher energy, and the shape gets closer to symmetric, that is, becomes more Compton-like. However, all the spectra have two features in common; a sharp rise at around 12 eV which corresponds to the first ionization potential of valence shells (12.6 eV) of H_2O, and another edge at around 30 eV, which corresponds to the ionization energy of O 2s orbital (33.2 eV).[28] Thus under the experimental conditions employed here, binding energies can not be neglected; the observed scattering should be analyzed in terms of both energy transfer and momentum transfer.

$S(q,E)$ can be transformed to GOS by the use of Eqs. 1 and 2, and subsequently the Bethe surface can be constructed. The Bethe surface of liquid water viewed from two different directions is shown in Fig. 4. While Fig. 4a emphasizes the domain of large momentum transfer and large energy loss, Fig. 4b emphasizes the domain of small momentum transfer and small energy loss. Also included in Fig. 4 is the result for gaseous water for q=0 by Chan et al.[27] obtained from EELS spectra with 1 eV resolution. A peak at 7.4 eV and a shoulder at 9.7 eV, both due to the excitation to bound excited states, and a sharp peak at 14 eV and a more intense but broad one at 20 eV followed by a long tail toward large energy loss are observed. Figure 4b shows that, with increasing momentum transfer, the optical features observed by EELS for q=0 are gradually smeared out and a broad ridge disperses to high energy loss.

Comparison of Liquid Phase GOS with Gas Phase GOS. Now we have GOS values of liquid water over a fairly wide range of q as well as E. Since Lassettre and White[5] have reported the GOS of gas phase water at several energies, it is possible to compare the liquid phase GOS with the gas phase one, as is shown in Fig. 5. It is evident from the figure that the two measurements agree quite well in absolute scale with each other. It is rather surprising, considering

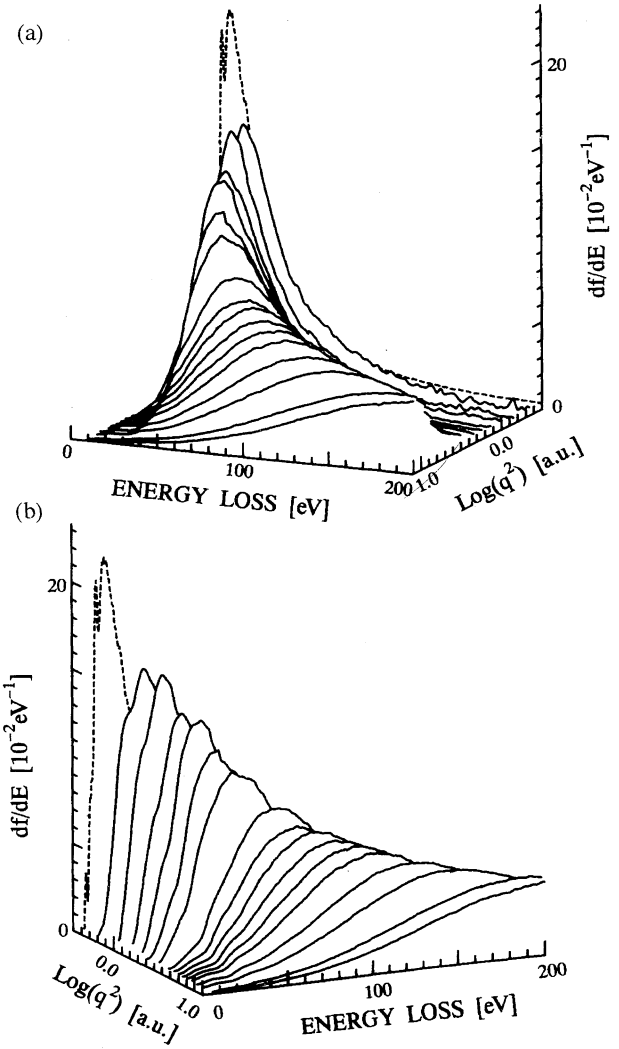

Fig. 4. Bethe surface of liquid water viewed from two different directions. Dots are for gas phase water at q=0 drawn from Table 1 of Ref. 27.

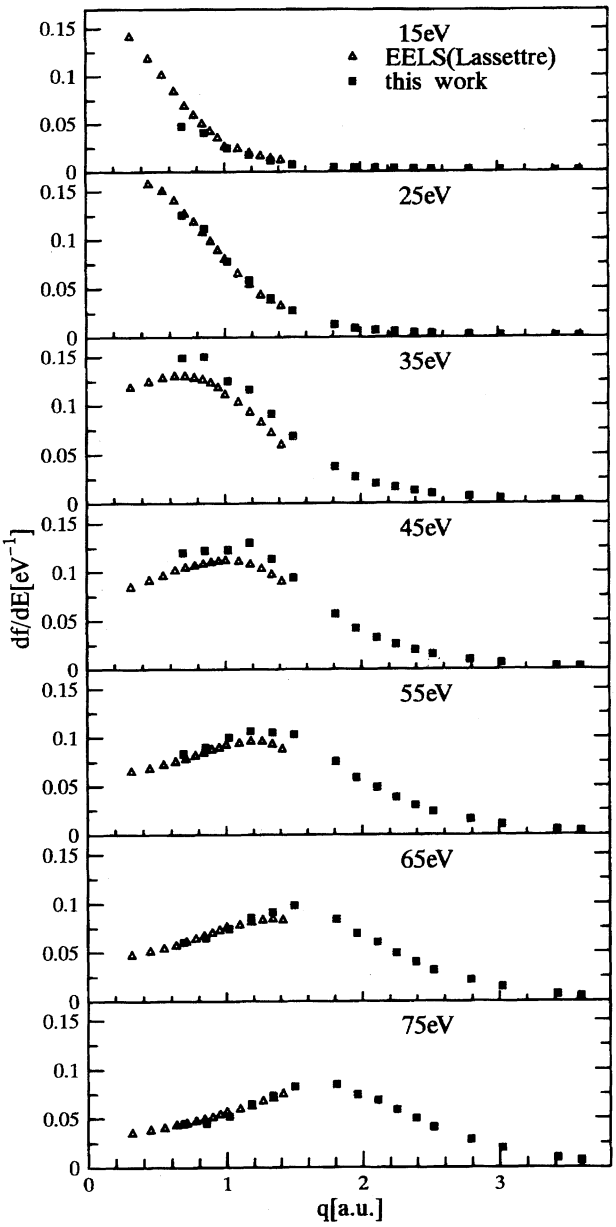

Fig. 5. Comparisons of the GOS determined by the present experiment with those for gas phase water drawn from Table IV of Ref. 5.

that they are derived from completely different experimental techniques and analytical procedures; one is EELS on the gas phase molecule and the elastic scattering intensities were employed to normalize the data, while the other is IXSS on liquid water and normalization is made using the Bethe sum rule. Slight discrepancies are, however, observed for energy losses of 35 and 45 eV; our data are systematically higher by 10—20%. It is not clear whether the difference should be attributed to experimental errors or not.

From the observations above, it can be concluded that the GOS of liquid water in the q–E range studied is determined by individual molecular properties and is little affected by intermolecular interactions. However, optical absorption spectra of gas phase molecules, which are the GOS at q=0, are often different from those in the liquid phase.[30] For example, Heller et al.[31] studied optical properties of liquid water in the vuv region through reflectance measurements. They observed a peak at around 21 eV which does not exist in the absorption spectra of water vapor and identified the peak as due to a collective electronic excitation. Kutcher and Green[32] proposed a model to describe GOS of liquid water, in which for small momentum transfer the GOS is dominated by the energy loss spectrum of liquid, while for large momentum transfer the GOS is given by gas phase values. The critical momentum q_c, beyond which collective excitations are no longer well-defined, was chosen to be 0.81 a.u. The observations here and those of Heller et al. are in line with their discussion except for the value of q_c, but a precise determination of the q_c is out of the scope of the present study.

Dielectric Response Function. The imaginary part of the inverse dielectric response function, called the loss function, is directly related to $S(q,E)$ by Eq. 4:[17]

$$\mathrm{Im}\frac{1}{\varepsilon(q,E)} = -\frac{4\pi^2 e^2 n}{\hbar(qa_0)^2}S(q,E). \tag{4}$$

Here n is the density of the molecule. The real part of the dielectric response function can then be calculated through the well-known Kramers–Kronig transformation, Eq. 5:

$$\mathrm{Re}\frac{1}{\varepsilon(q,E)} = 1 + \frac{2}{\pi}\wp\int_0^\infty E'\mathrm{d}E'\frac{\mathrm{Im}[\varepsilon^{-1}(q,E')]}{E'^2 - E^2}. \tag{5}$$

Figure 6 shows the loss function and the real (ε_1) as well as the imaginary (ε_2) part of the dielectric response function of liquid water. Although it is well known that the dielectric response function depends both on the energy and momentum transferred, few experimental determinations have been reported.[22,29]

No evidence of any existence of collective excitations has been suggested from the dielectric response function in the momentum transfer range studied here. It is well known that plasma excitation manifests themselves by a conspicuous peak of $\mathrm{Im}[-1/\varepsilon(q,E)]$ at the plasma frequency, and that ε_1 approaches zero at the same energy.[30] At the smallest q value studied here, namely 0.69 a.u., $\mathrm{Im}[-1/\varepsilon(q,E)]$ has a broad peak at around 20 eV, but ε_1 is far from zero; thus there are no indications of plasma excitation. Measurements at smaller q values may, however, reveal an existence of collective excitations in a molecular liquid. Unfortunately, under the present experimental conditions, parasitic scatterings have prevented us from obtaining any data at smaller q values.

Static Structure Factor. The static structure factor, $S(q)$, is defined by Eq. 6 and is known to be a very correlation sensitive quantity, as is evident from Eq. 7.[33]

$$S(q) = \int_0^\infty S(q,E)\mathrm{d}E \tag{6}$$

$$= \left\langle \int\int \Gamma(\boldsymbol{r}_1,\boldsymbol{r}_2)\exp[i\boldsymbol{q}\cdot(\boldsymbol{r}_1-\boldsymbol{r}_2)]\mathrm{d}\boldsymbol{r}_1\mathrm{d}\boldsymbol{r}_2 - |F(\boldsymbol{q})|^2 \right\rangle_\Omega + N, \tag{7}$$

$$F(\boldsymbol{q}) = \int \rho(\boldsymbol{r})\exp(i\boldsymbol{q}\cdot\boldsymbol{r})d\boldsymbol{r}. \tag{8}$$

Here $\rho(\boldsymbol{r})$ denotes the one electron density (normalized to N), the $\Gamma(\boldsymbol{r}_1,\boldsymbol{r}_2)$ the two electron density (normalized to $N(N-1)$), $F(\boldsymbol{q})$ the elastic scattering factor, and $\langle\cdots\rangle_\Omega$ the spherical average. The $S(q)$ derived by the use of Eq. 6 is tabulated in Table 1. Since the O 1s contribution is not taken into account in the measurement, calculated values according to Thakkar and Smith's formula[34] are added to make comparisons with theoretical calculations. Because the core contributions are small, less than 5% over the present q–E range, any error in the estimate of the core contribution is not significant. Since GOS is a normalized quantity, $S(q)$ determined in this manner is very precise. $S(q)$ is not only a measure of inelastic scattering intensities but also contains information about the electron–electron pair distribution and can be used to check the accuracy of wavefunctions, as long as reliable measurements are made.

Angle dependences of X-ray and electron scattering intensities from water have attracted attention of several investigators in the past. Shibata et al.[35] measured the momentum transfer dependence of the elastic and total differential cross

Table 1. Experimental $S(q)$ Values of Liquid Water
The O 1s contributions were calculated by means of the Thakkar & Smith's formula.[34]

	$S(q)$		
	Valence electrons		
q (a.u)	(Experimental)	O 1s	Total electrons
0.69	1.28	0.02	1.30
0.85	1.86	0.02	1.88
1.02	2.34	0.03	2.37
1.18	3.00	0.05	3.05
1.34	3.50	0.06	3.56
1.50	3.97	0.07	4.04
1.81	4.80	0.11	4.91
1.96	5.02	0.13	5.15
2.11	5.53	0.15	5.68
2.25	5.85	0.16	6.01
2.39	6.19	0.19	6.38
2.52	6.38	0.21	6.59
2.79	6.96	0.25	7.21
3.02	7.25	0.29	7.54
3.42	7.69	0.36	8.05
3.59	7.69	0.39	8.08

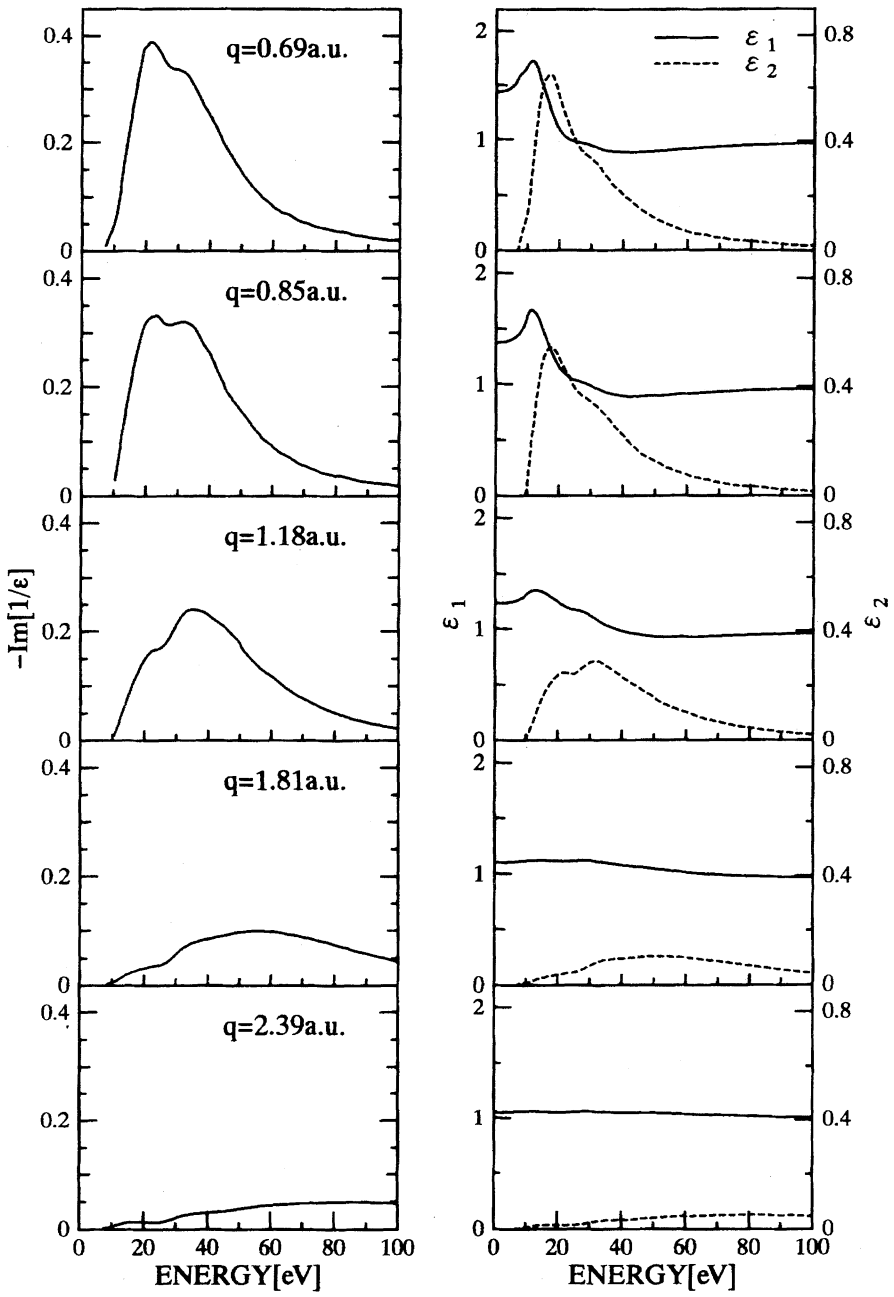

Fig. 6. q-Dependence of the loss function $\mathrm{Im}[-1/\varepsilon(q,E)]$ and the real (ε_1) as well as the imaginary (ε_2) part of the dielectric response function of liquid water.

sections for high energy electron scattering over a wide range of momentum transfer. They found that the elastic scattering cross sections by SCF MO calculation were in good agreement with their experiments. On the other hand, the calculated values for the total cross section by the independent atom model (IAM) deviate substantially from the experimental ones. Later, M. Takeuchi et al.[36] developed a computer program named ELIC to calculate elastic as well as inelastic electron scattering intensity by SCF-CI method, where all single and double excitation were included in the CI calculation. The calculated total (elastic+inelastic) differential cross sections were in good accordance with their experimental results. Very recently, H. Takeuchi et al.,[37] using SR as an excitation source, observed total X-ray scattering intensities over a range $0.74<q<5.0$ Å^{-1} and successfully analyzed the results in terms of the calculations by ELIC.

In all the studies described above, total or elastic scattering intensities have been the main concern. While the elastic scattering intensity bears information about the charge distribution in the system, the inelastic part contains the information about the electron–electron pair correlation, as is evident in Eqs. 7 and 8. It is thus preferable to extract inelastic scattering contribution separately to compare with theoretical calculations including correlation effects. Since in the present experiment the inelastic scattering intensities are singled out, the results offer a very sound ground to judge

whether or not electron correlation effects are properly taken into account in the wavefunctions used. Figure 7 compares various theoretically calculated static structure factors with the observed values from inelastic scattering intensities.

The IAM has generally been employed for analyses of X-ray diffraction studies.[38] Since static structure factors of various atoms have been calculated with Hartree–Fock (HF) wavefunctions,[39] $S(q)$ of molecules can easily be calculated within the IAM framework. The result is shown in Fig. 7. It is evident that the $S(q)$ of water by IAM-HF deviates significantly from the experimental one. A calculation using molecular HF wavefunction (MO-HF) has also been reported,[40] but there still exist notable discrepancies between the calculated and experimental $S(q)$ values. For convenience of comparisons, differences $\Delta S(q)$ obtained by subtracting $S(q)^{\mathrm{IAM-HF}}$ from various $S(q)$'s are shown in Fig. 8. $S(q)$ of several atoms, Li through Ar, have recently been calculated by Meyer et al.[33] In order to take electron correlation into consideration, they employed MR-SDCI (multi-reference singly and doubly excited CI) calculations (IAM-CI). As is evident in Figs. 7 and 8, a considerable deviation from the experimental values still exists even with the use of $S(q)$ calculated by IAM-CI.

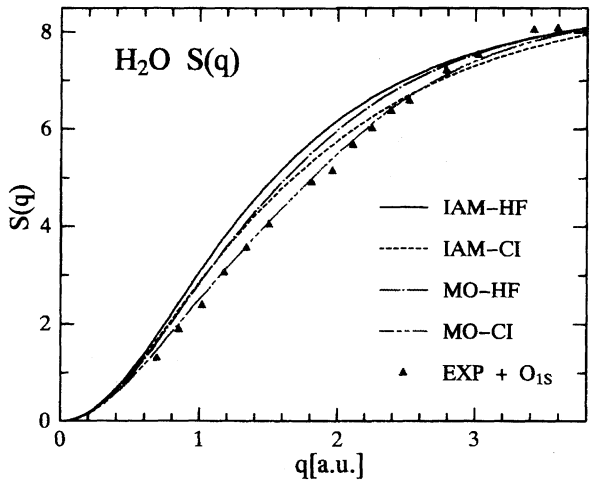

Fig. 7. A comparison of the observed $S(q)$'s with various calculations.

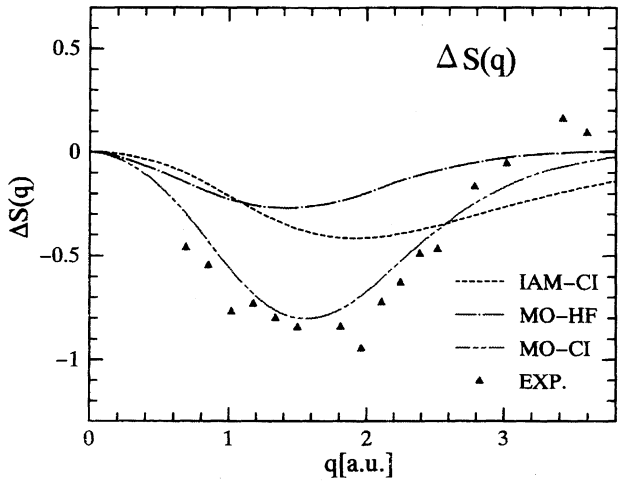

Fig. 8. Difference of various $S(q)$ from $S(q)^{\mathrm{IAM-HF}}$: $\Delta S(q)$.

Very recently Wang et al.[41] carried out detailed calculations on elastic as well as inelastic X-ray scattering intensities on a series of 10 electron molecules including H_2O. They have tabulated results obtained by using double zeta augmented with both the polarization and the diffuse functions (DZP++) for IAM, molecular HF, and CI including all single and double excitations (SDCI). They found that, while elastic scattering intensities do not differ very much between HF and CI levels, inelastic scattering intensities are very sensitive to the inclusion of CI. Figures 7 and 8 also show their SDCI results (MO-CI) by the use of DZP++. It is immediately clear that their calculation shows very good agreement with the experimentally observed $S(q)$. In Fig. 7, observed points are along the $S(q)^{\mathrm{MO-CI}}$ curve, and in Fig. 8 overall shapes are similar and the position of the extrema almost coincides. Although experimental values are a little deeper in Fig. 8, it may be considered to be within experimental errors.

From the results obtained here the following conclusions can be derived. First, it is necessary to take electron correlation effects properly into consideration in order to evaluate X-ray inelastic scattering intensities. In other words, X-ray incoherent scattering factors $S(q)$ can be a crucial test to judge the quality of wavefunctions. Second, the agreement of the experimentally derived $S(q)$ with the elaborate calculation including correlation, together with the fact that observed GOS coincides very well with the one derived from EELS, indicates that the accuracy obtained in the present IXSS experiment is quite satisfactory. Now experimental as well as theoretical studies on IXSS of several other liquids are in progress.

This experiment was carried out at the Photon Factory under the Proposal No. 95-G331. The authors are grateful to Prof. H. Kawata and Dr. K. Takeshita who are in charge of BL16A. We also thank Prof. S. Konaka and Dr. H. Takeuchi of Hokkaido Univ. for supplying us with the program ELIC.

References

1) M. Inokuti, *Rev. Mod. Phys.*, **43**, 297 (1971).
2) M. Inokuti, Y. Itikawa, and J. E. Turner, *Rev. Mod. Phys.*, **50**, 23 (1978).
3) R. A. Bonham and M. Fink, "High Energy Electron Scattering," Van Nostrand, London (1974).
4) M. A. Coplan, J. H. Moore, and J. P. Doering, *Rev. Mod. Phys.*, **66**, 985 (1994).
5) E. N. Lassettre and E. R. White, *J. Chem. Phys.*, **60**, 2460 (1974).
6) E. N. Lassettre and A. Skerbele, *J. Chem. Phys.*, **60**, 2464 (1974).
7) R. C. Ulsh, H. F. Wellenstein, and R. A. Bonham, *J. Chem. Phys.*, **60**, 103 (1974).
8) T. C. Wong, J. S. Lee, H. F. Wellenstein, and R. A. Bonham, *Phys. Rev. A*, **12**, 1846 (1975).
9) A. Lahman-Bennani, A. Duguet, and H. F. Wellenstein, *Chem. Phys. Lett.*, **60**, 405 (1979).
10) A. Lahman-Bennani, A. Duguet, H. F. Wellenstein, and M.

Rouault, *J. Chem. Phys.*, **72**, 6398 (1980).
11) S. N. Ketkar and R. A. Bonham, *Int. J. Quantum Chem.*, **20**, 627 (1986).
12) R. S. Barbieri and R. A. Bonham, *Phys. Rev. A*, **44**, 7361 (1991).
13) R. S. Barbieri and R. A. Bonham, *Phys. Rev. A*, **45**, 7929 (1992).
14) J. F. Ying and K. T. Leung, *J. Chem. Phys.*, **100**, 7120 (1994).
15) J. F. Ying and K. T. Leung, *J. Chem. Phys.*, **101**, 8333 (1994).
16) J. F. Ying and K. T. Leung, *Phys. Rev. A*, **53**, 1476 (1996).
17) C. Kittel, "Quantum Theory of Solids," John Wiley & Sons, New York (1963).
18) B. Williams, "Compton Scattering," McGraw-Hill, London (1977).
19) K. Tohji and Y. Udagawa, *Phys. Rev. B*, **36**, 9410 (1989).
20) K. Tohji and Y. Udagawa, *Phys. Rev. B*, **39**, 7590 (1989).
21) N. Watanabe, H. Hayashi, Y. Udagawa, K. Takeshita, and H. Kawata, *Appl. Phys. Lett.*, **69**, 1370 (1996).
22) W. Schulke, U. Bonse, H. Nagasawa, A. Kaprolat, and A. Berthold, *Phys. Rev. B*, **38**, 2112 (1988).
23) W. Schulke, J. R. Schmitz, H. Schulte-Schrepping, and A. Kaprolat, *Phys. Rev. B*, **52**, 11721 (1995).
24) W. Schulke, H. Nagasawa, S. Mourikis, and P. Lanzki, *Phys. Rev.*, **33**, 6744 (1983).
25) W. Schulke, H. Schulte-Schrepping, and J. R. Schmitz, *Phys. Rev. B*, **47**, 12462 (1993).
26) T. Matsushita, H. Maezawa, T. Ishikawa, M. Nomura, A. Nakagawa, A. Mikuni, Y. Muramatsu, Y. Satow, T. Kosuge, S. Sato, T. Koide, N. Kanaya, S. Asaoka, and I. Nagakura, *Rev. Sci. Instrum.*, **60**, 1874 (1989).
27) W. F. Chan, G. Cooper, and C. E. Brion, *Chem. Phys.*, **178**, 387 (1993).
28) K. H. Tan, C. E. Brion, Ph. E. van der Leeuw, and M. J. van der Wiel, *Chem. Phys.*, **29**, 299 (1978).
29) R. S. Barbieri and R. A. Bonham, *Mol. Phys.*, **77**, 1055 (1992).
30) M. Inokuti, *Radiat. Eff. Defects Solids*, **117**, 143 (1991).
31) J. M. Heller, R. N. Hamm, R. D. Birkhoff, and L. R. Painter, *J. Chem. Phys.*, **60**, 3483 (1974).
32) G. J. Kutcher and A. E. S. Green, *Radiat. Res*, **67**, 408 (1976).
33) H. Meyer, T. Muller, and A. Schweig, *Chem. Phys.*, **191**, 213 (1995).
34) A. J. Thakkar and V. H. Smith, *J. Phys. B*, **11**, 3803 (1978).
35) S. Shibata, F. Hirota, N. Kakuta, and T. Muramatsu, *Int. J. Quanatum Chem.*, **18**, 281 (1980).
36) M. Takeuchi, M. Nagashima, K. Tanaka, S. Konaka, and M. Kimura, *Int. J. Quantum Chem.*, **30**, 821 (1986).
37) H. Takeuchi, M. Nakagawa, T. Saito, T. Egawa, K. Tanaka, S. Konaka, and T. Mitsuhashi, *Int. J. Quantum Chem.*, **52**, 1339 (1994).
38) M. Kakudo and N. Kasai, "X-Ray Diffraction by Polymers," Kodansha, Tokyo (1972).
39) C. Tavard, D. Nicolas, and M. Rouault, *J. Chim. Phys.*, **64**, 540 (1967).
40) M. Kumar, A. N. Tripathi, and V. H. Smith, Jr., *Int. J. Quantum Chem.*, **29**, 1339 (1986).
41) J. Wang, A. N. Tripathi, and V. H. Smith, Jr., *J. Chem. Phys.*, **101**, 4842 (1994).